nature communications

Article

https://doi.org/10.1038/s41467-025-67312-4

High aspect ratio organic light-emitting diodes

Received: 15 June 2025

Accepted: 27 November 2025

Published online: 14 December 2025

Check for updates

Binyu Wang[1], Naresh B. Kotadiya[2], Taehwan Kim[3], Ryan Mashack[4], Dustin Comfort[4], Chao Huang[5], Claire E. Arneson[6], Marina Kondakova[4], Noel C. Giebink[2] ✉ & Max Shtein[5] ✉

Reliability is particularly challenging for organic light-emitting diodes (OLEDs) used in solid-state lighting applications, because OLED lifetime is inversely proportional to luminance, and most lighting applications demand high luminance. Here we introduce a strategy to overcome this tradeoff by constructing OLEDs on a substrate with sub-mm, high aspect ratio surface texture. By creating more active OLED area per unit lighting panel area, the device current density required to generate a given panel luminance decreases. We validate this approach for fluorescent and phosphorescent OLEDs, demonstrating good thickness uniformity on corrugated substrates with area enhancement factors up to 1.4x using a standard thermal evaporator. Relative to planar controls at the same panel current density, the high aspect ratio devices achieve a 2.7-fold increase in operating lifetime and up to a 40% increase in external light extraction efficiency, indicating that this approach offers a powerful pathway to improve the efficiency and lifetime of OLED lighting.

Organic light-emitting diodes (OLEDs) are widely used in mobile displays and flat panel televisions[1–3], but have yet to penetrate the general lighting market[4]. One challenge unique to OLED lighting stems from the fact that lighting applications require roughly an order of magnitude higher luminance than displays[5]. Because OLED efficiency[6] and operating lifetime[7] both decline with increasing current density (and thus luminance), it is especially difficult to meet the performance and lifetime targets set out for OLED lighting[8]. Improvements in optical outcoupling[9–14] and the use of tandem OLED stacks[15] are both beneficial from this standpoint, since they enable a given luminance to be achieved with lower current density. However, the current density reduction that can be achieved with these methods is limited, since outcoupling efficiency cannot exceed unity, and the number of stacks in a tandem OLED is limited to about six in practice[16].

Here, we introduce a new strategy to reduce OLED current density by constructing the device on a substrate with sub-mm, high aspect ratio surface texture. By creating more active OLED area per unit lighting panel area, the device current density required to generate a given panel luminance decreases. We demonstrate this approach using phosphorescent green and fluorescent blue OLEDs, and show that they can be fabricated with good thickness uniformity on corrugated substrates with area enhancement (AE) factors up to 1.4× using a standard vacuum thermal evaporation (VTE) coater. Green high aspect ratio devices can achieve the same luminance as a planar control at less than half the operating current density due to a combination of both area and outcoupling enhancement. Fade testing on the blue devices confirms that the AE is responsible for a 2.7-fold improvement in their operating lifetime relative to planar controls, indicating that the high aspect ratio approach is a viable pathway to improve the efficiency and lifetime of OLED lighting.

Results

Figure 1 illustrates the concept. Relative to a standard planar device, the same OLED layer stack on a triangular corrugated substrate with height-to-width aspect ratio, $\zeta = h/w$, has a larger active OLED area

[1]Department of Chemical Engineering, University of Michigan, Ann Arbor, MI, USA. [2]Department of Electrical Engineering and Computer Science, University of Michigan, Ann Arbor, MI, USA. [3]Department of Electrical Engineering, The Pennsylvania State University, University Park, PA, USA. [4]OLEDWorks LLC, Rochester, NY, USA. [5]Department of Materials Science and Engineering, University of Michigan, Ann Arbor, MI, USA. [6]Department of Physics, University of Michigan, Ann Arbor, MI, USA. ✉e-mail: ngiebink@umich.edu; mshtein@umich.edu

https://doi.org/10.1038/s41467-025-67312-4

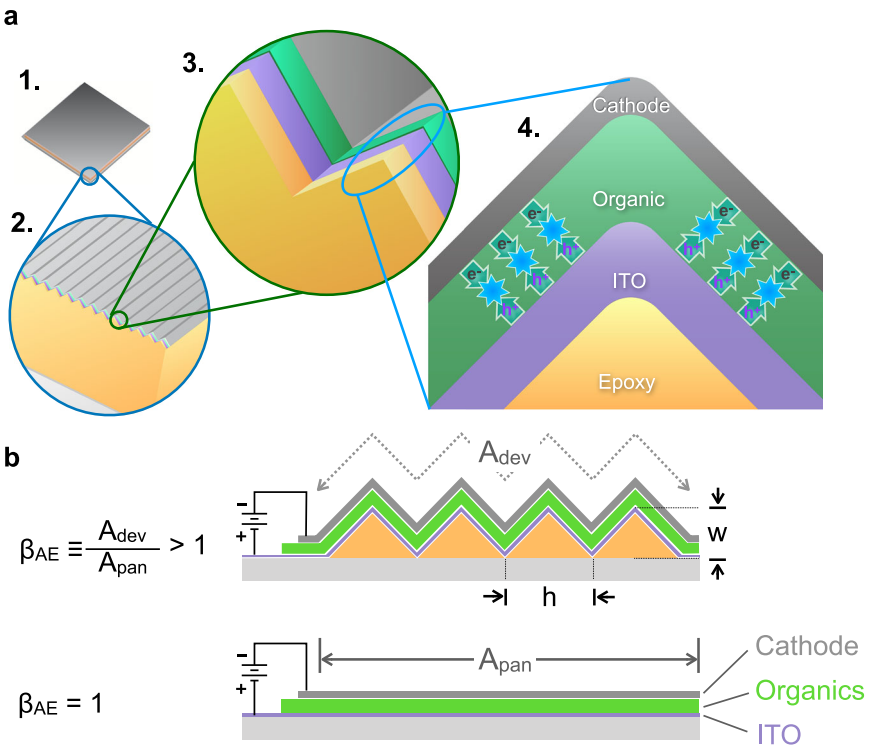

Fig. 1 | High aspect ratio OLED concept. a Device architecture shown at various length scales ranging from the panel level (1) to the nanoscale (4). **b** Fabricating a given OLED layer stack on a textured substrate allows for more active OLED area (A_{dev}) to be realized per unit panel area (A_{pan}), thereby reducing the device current density (J_{dev}) needed to achieve a given panel luminance (L_{pan}). The OLED is locally flat on the high aspect ratio substrate because the scale of the texture (~100 μm) is much larger than the OLED layer thickness (~100 nm), as emphasized in (**a**).

(A_{dev}) per unit panel area (A_{pan}) by a factor of $\beta_{AE} \equiv A_{dev}/A_{pan} = \sqrt{1+(2\zeta)^2}$. Thus, all other factors being equal, the high aspect ratio device can achieve the same panel luminance (L_{pan}) as its planar counterpart at lower current density, nominally by the same factor β_{AE}. We emphasize that this strategy differs from prior work employing nanoscale substrate corrugation for improved optical outcoupling, where $\zeta \ll 0.1$ and β_{AE} is negligible[17–19], or β_{AE} is not quantified[20,21]. Here, the 10–100 μm scale of the substrate texture is chosen to be much larger than the thickness of the OLED stack (so that the OLED can be considered locally planar from an electrical standpoint) while also being smaller than the visual acuity of the human eye (such that the panel luminance is perceived as spatially uniform).

To test this concept, we fabricate proof-of-concept high aspect ratio devices on corrugated substrates using the replication molding process outlined in Fig. 2. Briefly, polydimethylsiloxane (PDMS) molds are cast using commercially available microprism sheets (e.g., brightness-enhancing film for automotive applications[22]) with $0.2 < \zeta < 0.8$ and periods ranging from 10 to 100 μm. Then, ultraviolet (UV)-curable epoxy is poured onto the textured PDMS molds and the glass substrate is placed on top and cured (Fig. 2c); technical data for the epoxy resin is provided in Supplementary Note 1. The PDMS mold is subsequently peeled off, yielding the epoxy-on-glass high aspect ratio substrate (Fig. 2d). The refractive index of the cured epoxy is approximately equal to that of the glass and thus Fresnel reflection at the internal epoxy/glass interface is negligible.

Depositing an OLED layer stack with uniform thickness and no hot spots (i.e., locally thinner regions that could lead to shorting) is the key challenge for fabricating a high aspect ratio device. In this study, the indium-tin-oxide (ITO) anode is deposited by radio frequency (RF) sputtering (Fig. 2e) and the rest of the OLED stack is deposited by standard VTE (Fig. 2f). Note that, due to the directional nature of VTE

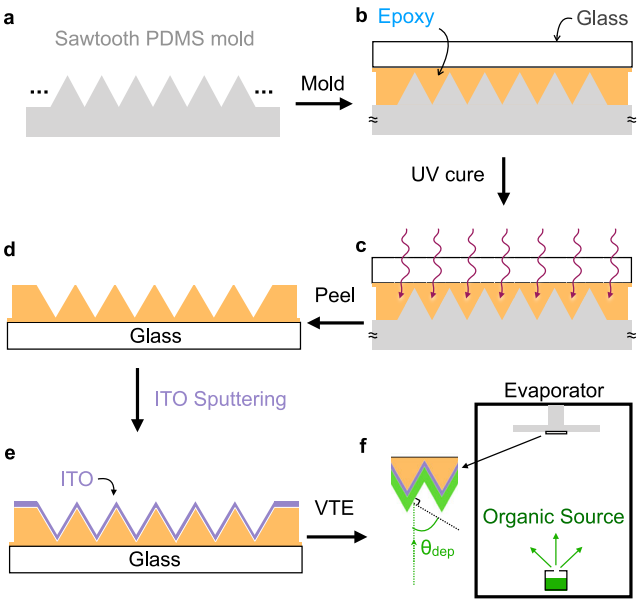

Fig. 2 | High aspect ratio OLED fabrication process. A corrugated PDMS mold (**a**) is replicated using ultraviolet-curable adhesive on glass (**b**, **c**) and then peeled off to yield the high aspect ratio substrate (**d**). A conformal ITO anode is subsequently deposited by sputtering (**e**), and then the organic layer stack is deposited by vacuum thermal evaporation (**f**).

and the off-normal local deposition angle highlighted in Fig. 2f, the nominal thickness of the organic layers must be increased by a factor of $[\cos(\theta_{dep})]^{-1} = \beta_{AE}$ relative to a planar reference device to maintain the same thickness along the local substrate normal direction.

https://doi.org/10.1038/s41467-025-67312-4

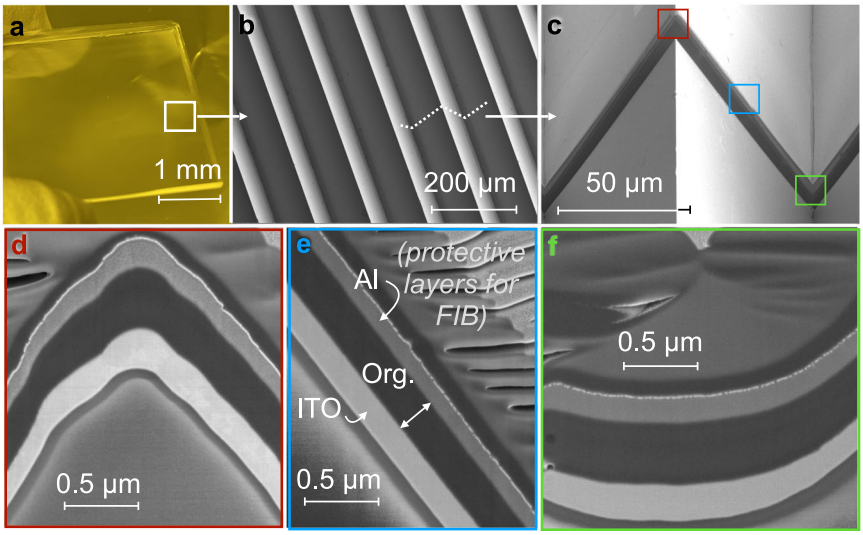

Fig. 3 | Coating uniformity on high aspect ratio substrates. a Photograph of a typical high aspect ratio substrate ($\beta_{AE} = 2$), along with scanning electron micrographs of the surface texture at progressively smaller scales (**b**, **c**). Cross-sectional images in (**d**–**f**) show the thickness profile of a mock OLED layer stack at the peak, side, and valley of the surface profile as indicated by the corresponding colored boxes along the focused ion beam cut in (**c**). The organic layer in this sample is tris(8-hydroxyquinolinato)aluminum (Alq_3); the white arrow in (**e**) is an example indicating the local thickness of this layer. The nonuniformity of the vertex feature shown in (**d**) results from imperfections in the master mold and is not due to thermal deformation during deposition of the ITO/Alq_3/Al layer stack.

Figure 3 presents the result of this process for a mock $\beta_{AE} = 2$ OLED, where the ITO, organic layer, and cathode (Al) thicknesses are measured via the scanning electron micrograph cross-sections in Fig. 3d–f. At the macroscale, the substrate texture is imperceptible and appears hazy to the naked eye (Fig. 3a); at the microscale, the triangular facets are smooth and free from defects (Fig. 3b). Since the peak and valley vertices of the corrugation are sharp (~0.5 μm radius of curvature), the planar facets account for the overwhelming majority of the OLED active area. The cross-sectional images show that the OLED layers are conformal, and that the peak (Fig. 3d) and valley (Fig. 3f) regions are locally thicker than the facets (Fig. 3e) as expected from the variation in local deposition angle[23]. Since increased OLED thickness generally leads to lower current at a given voltage, the vertex regions of the device are expected to be dimmer than the rest of the OLED, but crucially, should not be short-prone electrical hot spots.

Figure 4 examines the layer thickness uniformity in more detail for the same organic layer stack deposited on three different substrate corrugation geometries with AE factors ranging from $\beta_{AE} = 1.1$ to $\beta_{AE} = 2.0$. Figure 4b shows the variation in local thickness measured for each case. As expected from the local deposition angle (Fig. 2f), the thickness in the facet regions is less than in the vertex regions (at the edges and in the middle), roughly by a factor of β_{AE}^{-1} as shown in Fig. 4b. Hence, the nominal thickness, as measured by the quartz crystal microbalance in the deposition chamber, must be increased by a factor of β_{AE} to achieve the same local layer thickness as on planar devices. Focusing on these facet regions since they make up the majority of the active OLED area, we find that the thickness variation (standard deviation) relative to the mean is less than 5% in all cases.

Figure 5 shows that this level of thickness uniformity is sufficient to produce state-of-the-art green phosphorescent OLEDs. The thickness of each organic layer in the OLED stack is adjusted via β_{AE} to maintain the same facet thickness as a planar control device; full details of the device structure are provided in the Methods section. Figure 5a, b present photographs of the planar control, AE1.1, and AE1.4 corrugated devices along with their respective electroluminescence micrographs. The devices exhibit uniform emission except for the AE 1.1 case, where many dark spots are evident. These are attributed to a larger number of defects in the master mold used to produce the AE1.1 texture. The dimmer vertical stripes in the AE1.4 device correspond to the valley vertices of the corrugation pattern, where the thicker OLED layer stack conducts less current. The peak vertices are out of focus in this image and correspond to the thin bright lines between the dim vertical stripes. Functional AE2.0 devices were also fabricated, but these tended to fail quickly and were not reproducible.

Figure 5c shows the luminance-current-voltage characteristics for each device along with a second planar reference fabricated on commercial ITO. All of the devices exhibit comparably low shunt current at biases below ~2 V, indicating that pinholes or other leakage pathways on the textured substrates are negligible. The devices exhibit the same luminance turn-on voltage, though the planar commercial ITO device ultimately reaches higher current (and thus also luminance) due to its lower sheet resistance (14–15 Ω/sq for the commercial ITO compared to 20–25 Ω/sq for the in-house sputtered ITO). Small differences are observed in the EL spectra of the devices (Fig. 5d), possibly due to variation in the ITO and Al thickness (layers that were not corrected by β_{AE}) as well as multiple scattering due to the substrate texture. The angular emission profile measured in the plane orthogonal to the corrugation (Fig. 5d, inset) is close to Lambertian for all of the devices except for the AE1.1 case.

Figure 6a shows that the high aspect devices have significantly higher external quantum efficiency (EQE) than the planar controls. This is attributed to efficient outcoupling of substrate modes by scattering from the corrugated texture, since the OLED layer structure of each device (and thus the internal quantum efficiency) is nominally the same. Defining the outcoupling enhancement factor, β_{oc}, as the ratio of the high aspect device EQE to the planar control yields $\beta_{oc} \approx 1.6$ and $\beta_{oc} \approx 1.4$ for the AE1.1 and AE1.4 devices, respectively (Fig. 6a, right-hand axis). These enhancement factors are consistent with ray tracing simulations described in Supplementary Note 2. In both cases, the high aspect device outcoupling enhancement exceeds that achieved by applying an external light extraction film to a planar device (star symbols) and is comparable to the ~1.5× enhancement enabled by using a microlens array[9] or other scattering strategies[24,25].

Figure 6b presents the panel luminance (L_{pan}) versus J_{dev} for each device, highlighting the lower device current density needed for the high aspect devices to reach a luminance of 5000 cd m^{-2} compared with the planar controls. This reduction is due to the combined effect of outcoupling enhancement and AE. Higher β_{oc} means less current is

https://doi.org/10.1038/s41467-025-67312-4

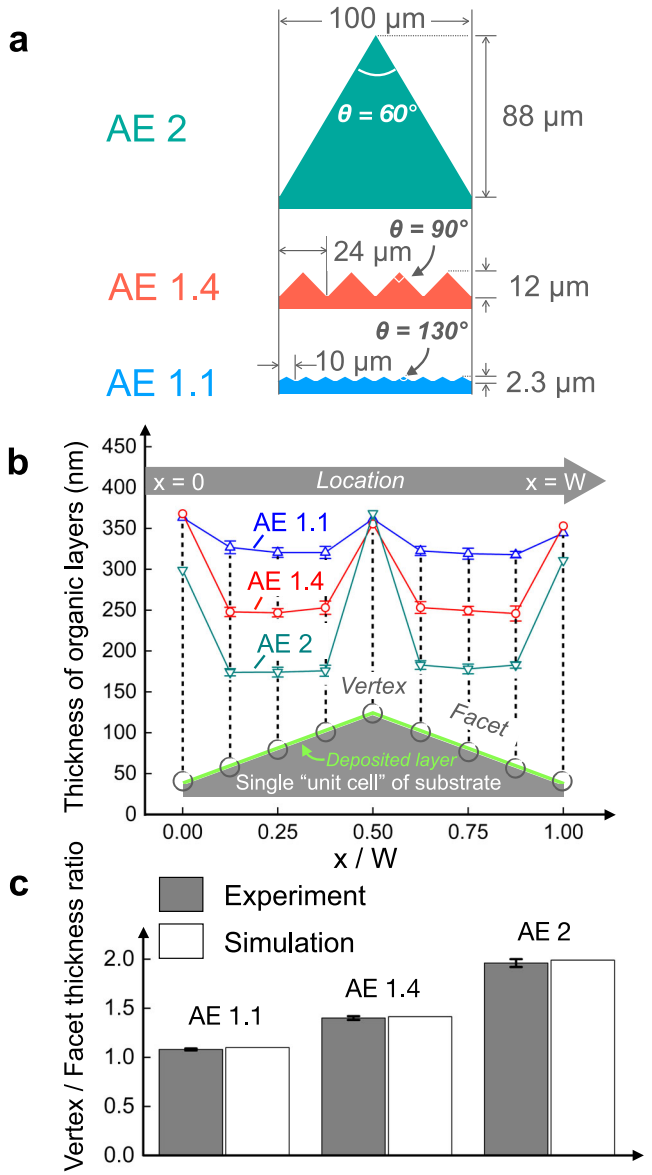

Fig. 4 | OLED thickness profile. a Three different high aspect ratio substrate geometries. **b** Local organic layer thickness measured (as in Fig. 3e) at nine different points over one period of the corrugation. The x-axis indicates the relative lateral position within one period. The average facet region thickness for the AE1.1, AE1.4, and AE2.0 structures is 321 ± 6 nm, 247 ± 6 nm, and 174 ± 6 nm, respectively, while the average thickness of the vertex regions is approximately 350 nm. **c** Comparison between the experimental vertex-to-facet thickness ratio and that expected based on the area enhancement factor β_{AE}. Error bars in (**b**) and (**c**) reflect ± one standard deviation from the mean.

required to produce a given light output, and higher β_{AE} means that this reduced current flows through a larger device active area, further decreasing the local current density. The total reduction factor in J_{dev} for a given panel luminance is therefore equal to the product, $\beta_{oc}\beta_{AE}$, in good agreement with the data as shown in Fig. 6c.

Similar improvements are observed for blue fluorescent OLEDs (see "Methods" for the device structure) fabricated on high aspect ratio substrates in Fig. 7. The EQE enhancement of the AE1.1 and AE1.4 devices in Fig. 7b is lower in this case compared with that of the green devices in Fig. 6 because the epoxy has parasitic absorption in the blue spectral region (owing to its UV-curable formulation; see Supplementary Note 3 for the transmission spectrum) that attenuates multiply-scattered light in the substrate. Figure 7c presents luminance fade results for the AE1.1, AE1.4 device and the commercial ITO planar control, demonstrating a 2.7-fold increase in LT95 lifetime (τ_{95}, defined as the time required to reach 95% of initial luminance) for the AE1.4 device. Note that the devices were aged at a constant panel current density of $J_{pan} = 3$ mA cm^{-2} (corresponding to an initial luminance of $L_0 \approx 200$ cd m^{-2} for the planar control devices) instead of constant panel luminance to avoid conflating changes in lifetime with changes in outcoupling efficiency. Fade measurements for the planar and high aspect ratio green devices are presented in Supplementary Note 4. The pre- and post-fade EL micrographs in Fig. 7c show that dark spots form over the course of aging in both the AE1.4 and commercial planar control devices. The fact that similar dark spots are observed in unfaded neighboring devices suggests that this is mainly a substrate cleanliness issue (i.e., the dark spots arise from particulate-induced pinholes) that is exacerbated in the AE device because of the additional processing steps used to create its texture.

Discussion

The luminance lifetime of OLEDs generally scales inversely with current density according to the empirical relationship, $\tau_{95} \propto J_{dev}^{-\alpha}$, where α ranges from 1.5 to 2.5[26,27]. The 2.7× lifetime enhancement observed for the AE1.4 device in Fig. 7c is therefore slightly larger than expected based only on its AE factor (i.e., a lifetime enhancement of $(\beta_{AE})^{\alpha}$). This might be related to differences in OLED temperature, which also affects the degradation rate[26] and is likely to be different for the planar and high aspect devices due to their different power dissipation densities ($\propto VJ_{dev} = VJ_{pan}\beta_{AE}^{-1}$) as well as different glass versus epoxy thermal conductivity; see Supplementary Note 5 for further discussion. Though a detailed understanding of the lifetime improvement mechanism requires additional experiments, Fig. 7c clearly shows that a prototype high aspect ratio OLED can exceed a state-of-the-art commercial control device. Given the similar lifetime enhancement observed for the green high aspect ratio OLEDs in Supplementary Note 4, it is reasonable to believe that the same improvement will ultimately translate to a stacked white device. Obviously, if the lifetime comparison were made at equal initial luminance, β_{oc} would contribute to an even larger lifetime enhancement. Though this outcoupling-related improvement in lifetime is trivial insofar as it occurs naturally for any light extraction strategy, it comes for free along with the β_{AE}-based improvement in high aspect ratio devices. In this context, it is worth emphasizing that, although the high aspect ratio approach is beneficial for lighting applications, it is probably not well-suited for displays, which would suffer from scattering-induced optical cross talk between pixels and image blur from the surface, as well as the basic problem of high-resolution pixel patterning on a textured substrate.

In principle, β_{AE} can be arbitrarily large, but in practice, it becomes difficult to deposit the OLED stack with sufficient uniformity to avoid pinholes and hotspots on substrates with aspect ratio $\zeta > 1$ in a research-style thermal evaporation chamber. Optimizing the throw distance and method of substrate rotation (e.g., planetary motion) provides one path to improve the uniformity. Another is to use organic vapor phase deposition[28], which enables highly conformal coating of organic thin films[29] and has demonstrated the capability to fabricate high-performance OLEDs over large area[30]. In-line vacuum coating systems used in OLED manufacturing[31] may also facilitate conformal deposition on high aspect ratio substrates owing to their short throw distance and wide range of deposition angles as the substrate translates laterally over each linear source.

An important challenge moving forward is to develop a mature high aspect ratio substrate platform. Textured polymer films, such as the brightness-enhancing film used here, are already mass produced and could be used directly as substrates for OLED fabrication. However, at least currently, the standard substrate for OLED lighting products is glass because it is impermeable and can survive the high-

https://doi.org/10.1038/s41467-025-67312-4

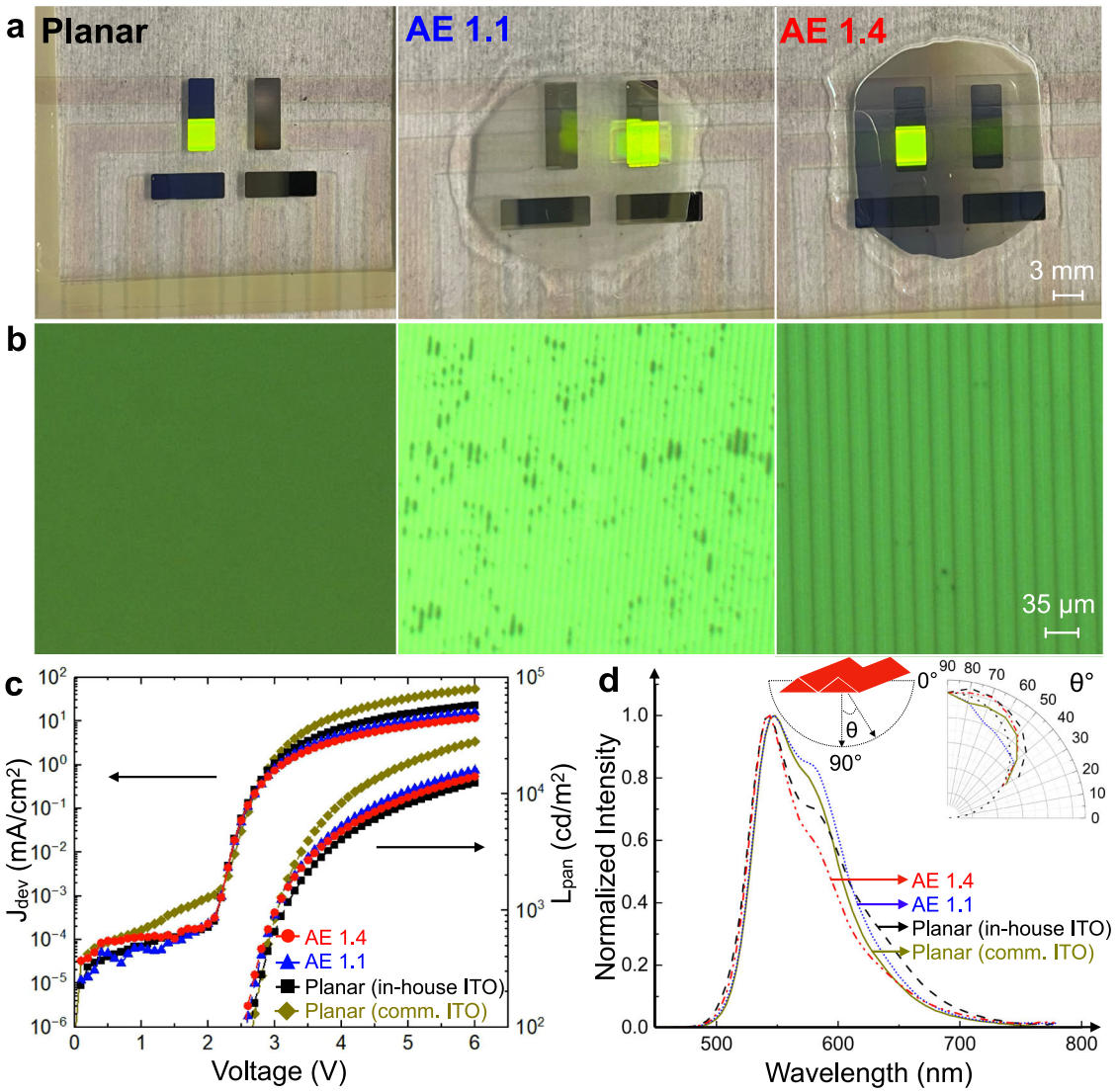

Fig. 5 | High aspect ratio phosphorescent OLEDs. a Photographs of lighted planar control, AE1.1, and AE1.4 green phosphorescent OLEDs. The corrugation of the AE1.1 and AE1.4 devices is oriented vertically, just as in the corresponding electroluminescence micrographs shown in (**b**). The lateral EL nonuniformity for the AE1.1 device in (**a**) results from waveguided light in the substrate that is slowly decoupled by scattering from the shallow surface texture. Brighter top and bottom edges of the adjacent AE1.4 device are due to edge effect-induced layer thickness variation from the shadow mask, which becomes more significant with increasing aspect ratio since the mask is forced farther away from the valleys of the substrate. **c** Luminance-current density (J_{dev})-voltage characteristics, including a planar device with standard commercial ITO for reference. **d** Electroluminescence spectra for the four devices, along with their angular emission profiles shown in the inset. The dotted line indicates an ideal Lambertian emission profile for reference.

temperature commercial ITO coating process. Etching[32], molding[33], direct embossing[34], and sol-gel molding[35] are all potential pathways to realize high aspect ratio glass substrates that could serve as a drop-in replacement in existing OLED manufacturing lines. Existing thin film encapsulation strategies are also compatible with high aspect ratio OLEDs since the ultra-barrier layer stacks are deposited conformally with techniques such as atomic layer deposition[36,37].

In summary, we have introduced high aspect ratio OLEDs as a path to improve device lifetime by reducing the local current density needed to achieve a given luminance. Proof-of-concept fluorescent and phosphorescent OLEDs with an AE factor of 1.4× demonstrate a 2.7-fold increase in lifetime and up to a 40% increase in external light extraction efficiency. Given that this approach is compatible with tandem OLEDs and can be implemented on existing production lines without changing the OLED formulation, it offers a versatile solution to overcome the efficiency and reliability challenges currently faced by OLED lighting technology.

Methods

Fabrication

Acrylic Fresnel prism sheets used for the AE1.1 texture are purchased from NTKJ CO., LTD., Japan while the AE1.4 texture is replicated from 3M brightness enhancement films (BEF4-GT-90(24)-Auto) purchased from American Polarizers Inc. PDMS (Sylgard 184) is mixed at a 10:1 ratio, degassed, poured onto the master mold, and cured at 65 °C in an oven overnight. The PDMS is subsequently removed and UV-curable epoxy (OG−142-87, Epoxy Technology Inc.) is dispensed on the corrugated surface. A soda-lime glass substrate is then placed on top, smearing out the epoxy underneath, and the epoxy is cured by UV exposure through the glass for 14 min, resulting in a corrugated epoxy layer that is approximately 0.2 mm thick. A higher viscosity epoxy (OG-142) is then dispensed using a flat-tip needle around the edge of the pattern to bridge the step between the glass and the corrugated layer to facilitate continuity of the subsequent ITO contact. Finally, the glass/epoxy

https://doi.org/10.1038/s41467-025-67312-4

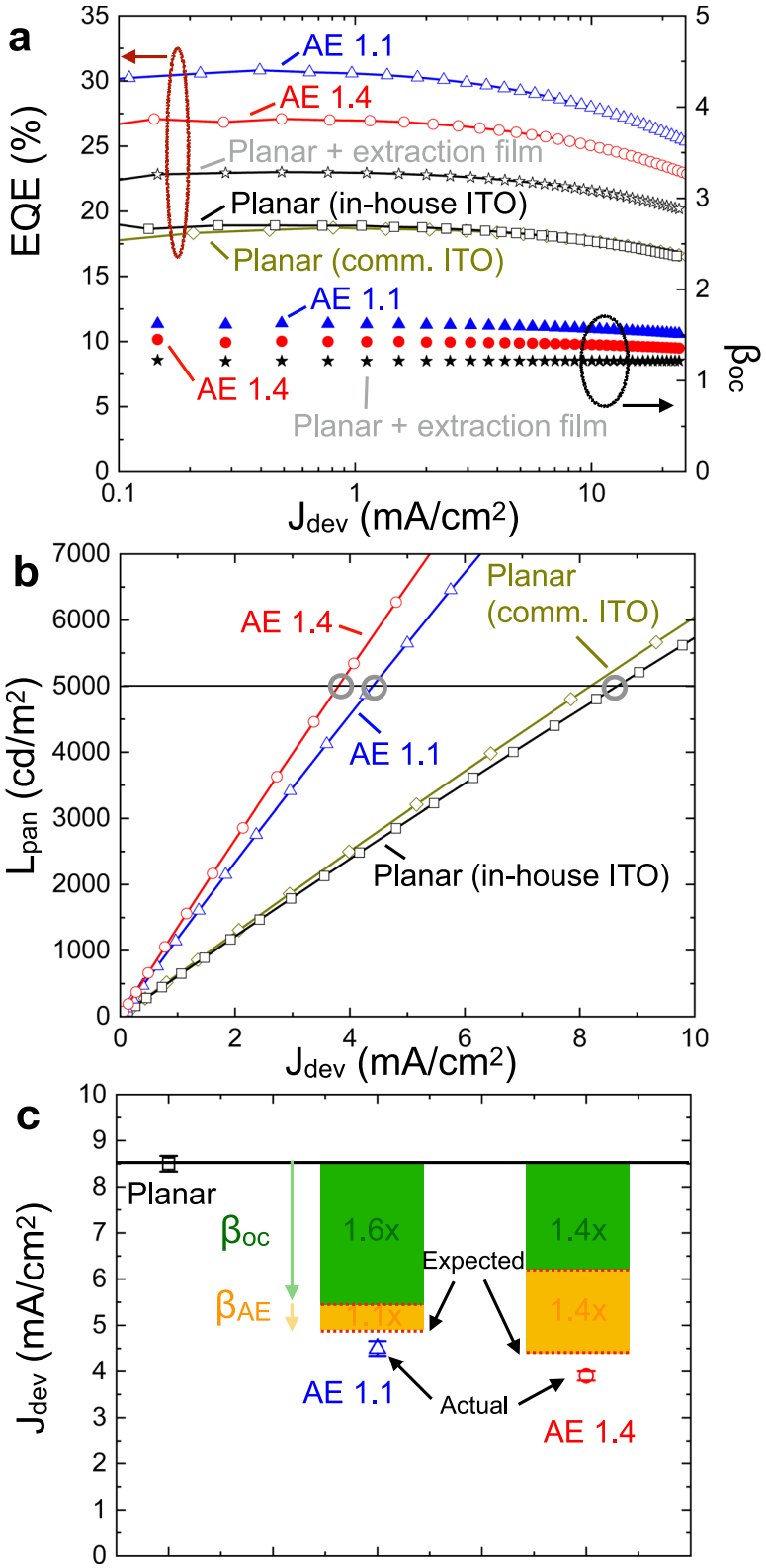

Fig. 6 | Green OLED performance. a External quantum efficiency (EQE) for each OLED as a function of device current density, J_{dev}, calculated as the total current divided by the active device area, A_{dev}. The star symbols represent a planar commercial ITO control device measured with an external light extraction film applied to its surface. The right-hand axis shows the EQE enhancement ratio of each device relative to the planar control. **b** Panel luminance versus device current density for each device. **c** Device current density (corresponding to the gray circles in (**b**)) required to achieve a panel luminance of 5000 cd m^{-2}. The green and yellow shaded bars break down the relative contributions of outcoupling enhancement (β_{oc}) and area enhancement (β_{AE}) to the reduction in J_{dev} relative to the planar control. Error bars on the data points in (**c**) reflect ± one standard deviation from the mean.

https://doi.org/10.1038/s41467-025-67312-4

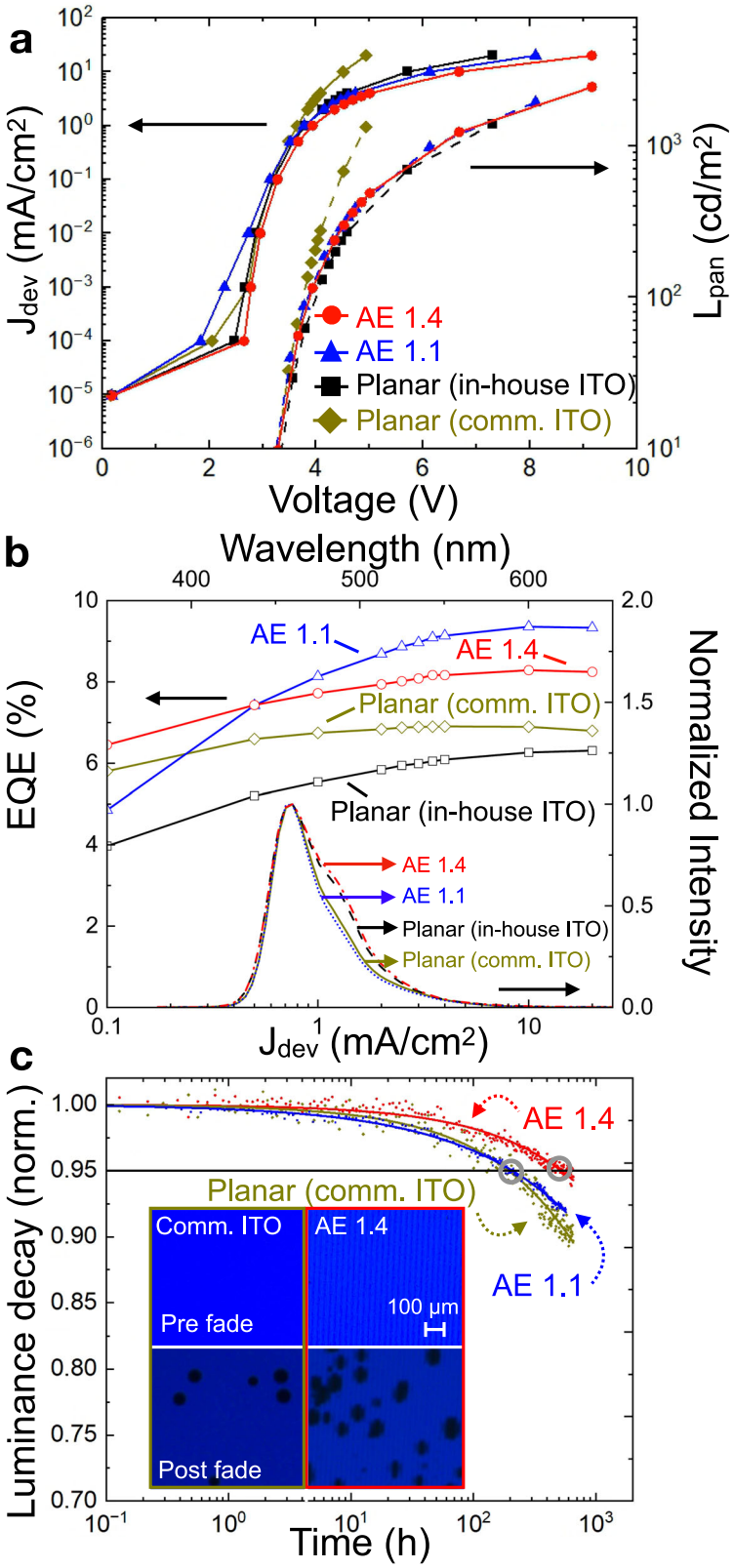

Fig. 7 | High aspect ratio lifetime enhancement. a Luminance-current density (J_{dev})-voltage characteristics for blue fluorescent devices fabricated on AE1.1, AE1.4, and planar substrates with commercial and in-house deposited ITO. **b** External quantum efficiency and EL spectra (inset) for the devices. **c** Luminance fade data for the AE1.1, AE1.4, and commercial ITO planar control devices at a constant panel current density of J_{pan} = 3 mA cm^{-2}. The solid lines are fits to an empirical stretched exponential model and are intended only as guides for the eye. The inset shows pre- and post-fade EL micrographs of both the AE1.4 and commercial planar control devices.

substrates are placed on a 120 °C hot plate for one hour to ensure that the epoxy is fully cured.

Indium-tin-oxide anode contacts are deposited via radio frequency (RF) sputtering in a top-down format, with the target positioned above the substrates at a slight angle. Following a brief clean with an ionized nitrogen gun, the substrates are placed onto a substrate holder with a shadow mask and then loaded into the deposition system on a heated stage at 100 °C. The ITO deposition is carried out using Ar at a flow rate of 50.0 sccm, a pressure of 5.0 mTorr, and an RF power of 400 W. Approximately 200 nm of ITO is deposited at an average rate of 1.6–1.7 Å/s. A witness sample is subsequently measured to determine the sheet resistance (Ω/sq), thickness, and optical density. The sheet resistance typically ranges between 20 and 25 Ω/sq and the transmittance is approximately 90%.

The OLEDs reported in this work were fabricated at OLEDWorks, LLC using commercial state-of-the art materials and a thermal evaporator with a base pressure of ~10^{-7} Torr. The materials used in the devices are proprietary but yield similar performance to published materials. They include a hole transport material (HTM), an electron blocking material (EBM), an electron transport material (ETM), and blue and green host materials (BH/GH) used for blue fluorescent and green phosphorescent dopants (BD/GD), respectively. The green phosphorescent OLED structure is ITO/60 nm hole injection layer (94% HTM, 6% p-dopant)/110 nm HTM/10 nm EBM/30 nm emissive layer (90% GH, 10% GD)/33 nm ETM/10 nm electron injection layer (98% ETM, 2% Li) followed by a 125 nm Al cathode. The commercial ITO green control device has a 100 nm Ag cathode instead. The blue fluorescent structure is similar: ITO/60 nm hole injection layer (94% HTM, 6% p-dopant)/296 nm HTM/10 nm EBM/20 nm emissive layer (94% BH, 6% BD)/23 nm ETM/10 nm electron injection layer (98% ETM, 2% Li)/125 nm Al. The Al thickness is not corrected for the textured substrate. The substrate holder rotates in the center of the chamber and the throw distance from the sources to the substrate holder is approximately 30 cm. Note that the textured substrates are placed in the substrate holder with their grooves oriented radially, which is important for uniform coating of the facets. All of the devices are encapsulated using Ajinomoto film and pocketed glass. The nominal active device area is 10 mm^2, though this can vary slightly for the high aspect ratio devices due to their texture and thus is determined for each device individually in an optical microscope.

Characterization

The devices are independently characterized using a SpectraScan PR655 spectroradiometer (OLEDWorks) and a Si photodiode with an integrating sphere (University of Michigan) to avoid error in the measured EQE that could result from their varying angular emission profiles. External light-extraction film used on some of the planar reference devices is purchased from American Polarizers Inc. The angular emission profile/spectrum is measured using an automated rotation stage and a fiber-coupled mini-spectrometer. All measurements are conducted at ambient temperature in a dark box. Luminance fade testing is carried out at OLEDWorks under constant current driving at a current density of 3 mA cm^{-2} defined by the lit area of each device measured using an optical microscope. A forced air flow of approximately 100 linear ft/min maintains the devices at 25 °C throughout the test.

Data availability

Source data are provided for all of the plots in this paper. The image data are available from the authors upon request. Source data are provided with this paper.

References

1. Park, C. I. et al. World's first large size 77-inch transparent flexible OLED display. *J. Soc. Inf. Disp.* **26**, 287–295 (2018).
2. Vieri, C. et al. An 18 megapixel 4.3" 1443 ppi 120 Hz OLED display for wide field of view high acuity head mounted displays. *J. Soc. Inf. Disp.* **26**, 314–324 (2018).
3. Kato, K. et al. 5,291-ppi OLED display enabled by monolithic integration of *C*-axis-aligned crystalline IGZO FET and Si CMOS. *J. Soc. Inf. Disp.* **30**, 690–698 (2022).
4. Kato, K., Iwasaki, T. & Tsujimura, T. Over 130 lm/W all-phosphorescent white OLEDs for next-generation lighting. *JPST* **28**, 335–340 (2015).
5. Spindler, J. et al. 24-2: *Invited Paper*: high brightness OLED lighting. *Dig. Tech. Pap. - SID Int. Symp.* **47**, 294–297 (2016).
6. Sun, Y. et al. Management of singlet and triplet excitons for efficient white organic light-emitting devices. *Nature* **440**, 908–912 (2006).
7. Spindler, J. P. et al. System considerations for RGBW OLED displays. *J. Soc. Inf. Disp.* **14**, 37–48 (2006).
8. U.S. Department of Energy. *2022 Solid-State Lighting R&D Opportunities* (Office of Energy Efficiency & Renewable Energy, Washington, D.C., 2022).
9. Möller, S. & Forrest, S. R. Improved light out-coupling in organic light emitting diodes employing ordered microlens arrays. *J. Appl. Phys.* **91**, 3324–3327 (2002).
10. Sun, Y. & Forrest, S. R. Enhanced light out-coupling of organic light-emitting devices using embedded low-index grids. *Nat. Photonics* **2**, 483–487 (2008).
11. Qu, Y., Slootsky, M. & Forrest, S. R. Enhanced light extraction from organic light-emitting devices using a sub-anode grid. *Nat. Photonics* **9**, 758–763 (2015).
12. Chang, H.-W. et al. Nano-particle based scattering layers for optical efficiency enhancement of organic light-emitting diodes and organic solar cells. *J. Appl. Phys.* **113**, 204502 (2013).
13. Afolayan, E. O. et al. Improved light extraction in organic light-emitting diodes via semiconductor dilution. *Adv. Opt. Mater.* **12**, 2302588 (2024).
14. Riedel, B., Kaiser, I., Hauss, J., Lemmer, U. & Gerken, M. Improving the outcoupling efficiency of indium-tin-oxide-free organic light-emitting diodes via rough internal interfaces. *Opt. Express* **18**, A631 (2010).
15. Kido, J. et al. 27.1: *Invited Paper*: high efficiency organic EL devices having charge generation layers. *Dig. Tech. Pap. - SID Int. Symp* **34**, 964–965 (2003).
16. Spindler, J. et al. 84-1: *Invited Paper*: advances in high efficacy and flexible OLED lighting. *Dig. Tech. Pap. - SID Int. Symp.* **49**, 1135–1138 (2018).
17. He, W., Zhou, J.-G., Sun, S.-Q. & Fung, M.-K. Island-like random scattering layer for light extraction in organic light-emitting diodes with enhanced luminous efficiencies and angular spectral stability. *Mater. Today Energy* **28**, 101068 (2022).
18. Altun, A. O. et al. Corrugated organic light emitting diodes for enhanced light extraction. *Org. Electron.* **11**, 711–716 (2010).
19. Lee, S. et al. Enhancement of light extraction efficiency and suppression of roll-off characteristics of thermally activated delayed fluorescence organic light-emitting diodes by inserting nanoscale pixel-defining layer. *Adv. Electron. Mater.* **9**, 2201264 (2023).
20. Zhu, W. et al. A simple effective method to improve light out-coupling in organic light-emitting diodes by introducing pyramid-based texture structure. *Org. Electron.* **15**, 1113–1119 (2014).
21. Hippola, C. et al. Enhanced light extraction from OLEDs fabricated on patterned plastic substrates. *Adv. Opt. Mater.* **6**, 1701244 (2018).
22. Bastawros, A., Zhou, J., Davis, M. & Chen, Z. *Advanced Optical Films for Automotive Displays 2011-01–0462* (SAE International, 2011).
23. Zhao, Y. et al. Effects of substrate topography on current injection and light emission properties of organic light emitting devices. *Org. Electron.* **15**, 3529–3537 (2014).
24. Shinar, R. & Shinar, J. Light extraction from organic light emitting diodes (OLEDs). *J. Phys. Photonics* **4**, 032002 (2022).

25. Koh, T.-W., Spechler, J. A., Lee, K. M., Arnold, C. B. & Rand, B. P. Enhanced outcoupling in organic light-emitting diodes via a high-index contrast scattering layer. *ACS Photonics* **2**, 1366–1372 (2015).
26. Forrest, S. R. *Organic Electronics: Foundations to Applications* (Oxford University Press, Oxford, 2020).
27. Tankelevičiūtė, E., Samuel, I. D. W. & Zysman-Colman, E. The blue problem: OLED stability and degradation mechanisms. *J. Phys. Chem. Lett.* **15**, 1034–1047 (2024).
28. Shtein, M., Gossenberger, H. F., Benziger, J. B. & Forrest, S. R. Material transport regimes and mechanisms for growth of molecular organic thin films using low-pressure organic vapor phase deposition. *J. Appl. Phys.* **89**, 1470–1476 (2001).
29. Yang, F., Shtein, M. & Forrest, S. R. Controlled growth of a molecular bulk heterojunction photovoltaic cell. *Nat. Mater.* **4**, 37–41 (2005).
30. Lunt, R. R., Lassiter, B. E., Benziger, J. B. & Forrest, S. R. Organic vapor phase deposition for the growth of large area organic electronic devices. *Appl. Phys. Lett.* **95**, 233305 (2009).
31. Spindler, J., Hamer, W. J. & Kondakova, E. M. OLED manufacturing equipment and methods. In *OLED Manufacturing, Equipment and Methods*. (eds Karlicek, R., Sun, C.C., Zissis, G. & Ma, R.) 417–441 (Springer, 2017).
32. Yin, Y. et al. Rapid fabrication of superhydrophobic and transparent surfaces by using laser-induced deep etching process. *Opt. Express* **32**, 35321 (2024).
33. Kotz, F. et al. Liquid glass: a facile soft replication method for structuring glass. *Adv. Mater.* **28**, 4646–4650 (2016).
34. Zhu, Z. et al. Novel roll-to-plate hot embossing process for the precision manufacturing of glass microstructures. *Ceram. Int.* **50**, 43089–43097 (2024).
35. Muromachi, T., Tsujino, T., Kamitani, K. & Maeda, K. Application of functional coatings by sol-gel method. *J. Sol-Gel Sci. Techn.* **40**, 267–272 (2006).
36. Hirvikorpi, T., Vähä-Nissi, M., Mustonen, T., Iiskola, E. & Karppinen, M. Atomic layer deposited aluminum oxide barrier coatings for packaging materials. *Thin. Solid Films* **518**, 2654–2658 (2010).
37. Wu, J. et al. Efficient multi-barrier thin film encapsulation of OLED using alternating Al_2O_3 and polymer layers. *RSC Adv.* **8**, 5721–5727 (2018).

Acknowledgements

This work was supported by the U.S. DOE Building Technologies Office under Award No. DE-EE0009694 (N.C.G., M.S., M.K.). The authors acknowledge the University of Michigan College of Engineering for financial support and the Michigan Center for Materials Characterization for use of the instruments and staff assistance.

Author contributions

N.C.G. and M.S. conceived the idea and supervised the project. B.W., N.B.K., R.M., D.C., and M.K. designed the experiments and fabricated and characterized the devices. C.H. and C.E.A. assisted with analysis and manuscript preparation. B.W. analyzed the data and T.K. assisted with modeling. B.W., N.C.G., and M.S. wrote the manuscript with revisions and approval from all of the authors.

Competing interests

R.M., D.C., and M.K. are employees of OLEDWorks, LLC, a company that manufactures OLED lighting products. The remaining authors declare no competing interests.

Additional information

Supplementary information The online version contains supplementary material available at https://doi.org/10.1038/s41467-025-67312-4.

Correspondence and requests for materials should be addressed to Noel C. Giebink or Max Shtein.

Peer review information *Nature Communications* thanks Jeong Hyun, Hirohiko Fukagawa, and the other anonymous, reviewer(s) for their contribution to the peer review of this work. A peer review file is available.